PHYSICAL REVIEW D VOLUME 9, NUMBER 3 1 FEBRUARY 1974

Inclusive production of K_1^0, Λ^0, and $\bar{\Lambda}^0$ in 18.5-GeV/c $\pi^{\pm}p$ interactions*

P. H. Stuntebeck,† N. M. Cason, J. M. Bishop, N. N. Biswas, V. P. Kenney, and W. D. Shephard
Department of Physics, University of Notre Dame, Notre Dame, Indiana 46556
(Received 16 August 1973)

Data are presented for the single-particle inclusive reactions $\pi^{\pm}p \to K_1^0 +$anything, $\pi^{\pm}p \to \Lambda^0 +$anything, and $\pi^{\pm}p \to \bar{\Lambda}^0 +$anything at 18.5 GeV/$c$. We have studied the invariant cross section $Ed^3\sigma/d\vec{p}$ in terms of the variables (P_L, P_T^2), (x, P_T^2), (y, P_T^2), and (y_r, P_T^2). The distributions for the longitudinal-momentum variable depend strongly on the type of particle produced. The K_1^0 distributions are not symmetric about $x=0$, where x is the Feynman scaling variable; more K_1^0's are produced in the forward hemisphere, suggestive of beam fragmentation. The Λ^0 distributions peak in the backward hemisphere, suggestive of target fragmentation. The $\bar{\Lambda}^0$ distributions are significantly different from the Λ^0 distributions. Distributions of transverse momentum are fitted with the function $Ae^{-BP_T^2}$. The average transverse momentum of the K_1^0, Λ^0, and $\bar{\Lambda}^0$ increases logarithmically with the mass of the produced particle. Topological cross sections and multiplicity distributions are presented. We have studied the Λ^0 polarization as a function of $|t-t_{\min}|$, x, and charge multiplicity. We find that the π^-p data show a significant polarization for $0.5 \le |t-t_{\min}| \le 1.5$ (GeV/c)^2 and for $-0.8 \le x \le -0.4$, while in the π^+p data the polarization is everywhere consistent with zero.

I. INTRODUCTION

Inclusive reactions of the type $a+b \to c+$anything have been studied for a variety of incident particles a and outgoing particles c. We have previously presented[1] results for 18.5-GeV/c $\pi^{\pm}p$ interactions in which the produced particle is a π^-. In this paper we present results for $\pi^{\pm}p$ reactions at the same incident momentum where the produced particle is a K_1^0, $\Lambda^0(\Sigma^0)$, or $\bar{\Lambda}^0(\bar{\Sigma}^0)$.[2] Specifically, we have studied the reactions

$$\pi^+p \to K_1^0 + \text{anything}, \quad (1)$$

$$\pi^-p \to K_1^0 + \text{anything}, \quad (2)$$

$$\pi^+p \to \Lambda^0 + \text{anything}, \quad (3)$$

$$\pi^-p \to \Lambda^0 + \text{anything}, \quad (4)$$

$$\pi^+p \to \bar{\Lambda}^0 + \text{anything}, \quad (5)$$

$$\pi^-p \to \bar{\Lambda}^0 + \text{anything}, \quad (6)$$

all at 18.5-GeV/c incident momentum. No data for reactions (2)–(6) have so far been presented in the literature; some data for reaction (1) at 6 and 22 GeV/c have been published.[3]

We examine the characteristics of the six inclusive processes and make comparisons with other strange-particle inclusive data. We present our data in terms of several sets of variables which we define in Sec. II. In Sec. III we discuss the experimental procedure used to obtain our data. This includes discussions of contamination, decay fiducial volume, resolution of ambiguities, and corrections to the data. In Sec. IV we present the topological cross sections and the charge multiplicity of events in which V^0's are produced.[4] In Sec. V we present and discuss the single-particle longitudinal-momentum distributions in the center-of-mass system for the K_1^0's, Λ^0's, and $\bar{\Lambda}^0$'s. We examine the target-fragmentation region for each of these three particles, compare the transverse-momentum-squared distributions and present fits to these distributions, and study the mean transverse momenta. We also present data on the polarization of the Λ^0's produced in these inclusive reactions.

II. DEFINITION OF VARIABLES

We have studied the inclusive-momentum spectra for reactions (1)–(6) in terms of several different variables. Single-particle inclusive reactions are characterized by the invariant differential cross section $f(\vec{p}, s) = Ed^3\sigma/d\vec{p}$, where s is the square of the total c.m. energy, $\vec{p}$ the momentum, and E the energy of the produced particle. For unpolarized beam and target we can express $f(\vec{p}, s)$ as a function of s and two other in-

dependent variables. We present in this paper distributions of $f(\vec{p}, s)$ in terms of the four sets of variables (P_L, P_T^2), (x, P_T^2), (y, P_T^2), and (y_r, P_T^2). Here P_L is the component of momentum along the direction of the beam in the laboratory frame; x is the Feynman scaling variable defined as $x = 2P_L^*/\sqrt{s}$, where the asterisk indicates c.m. quantity; y is the c.m. rapidity defined as

$$y = \tfrac{1}{2}\ln\left(\frac{E^* + P_L^*}{E^* - P_L^*}\right)$$

$$= \ln\left(\frac{E^* + P_L^*}{\mu}\right),$$

with $\mu = (P_T^2 + m^2)^{1/2}$; y_r is the reduced rapidity[5] defined as $y_r = 2y/Y$, with $Y = \ln(s/\mu^2)$; P_T^2 and m are the square of the transverse momentum and the mass of the produced particle, respectively.

The rationale for using these many different sets of variables stems from the desirability of comparing our data with many different theoretical models. Fragmentation models lead to predictions about the distributions of particles whose momenta remain finite in the rest frame of the target or projectile as $s \to \infty$. Thus the appropriate variables for the study of target fragmentation are P_L and P_T^2. Models which make predictions about the distributions of particles whose momenta remain finite in the over-all c.m. frame as $s \to \infty$ are better studied in terms of x and P_T^2. The rapidity variable y has the advantage of expanding the region near $x = 0$, thus allowing a detailed study of the central region. Rapidity may be evaluated in any reference frame; in this paper we present distributions as a function of c.m. rapidity. Rapidity has the added advantage that the distributions in all longitudinal frames are related by a simple translation along the rapidity axis. Reduced rapidity, also presented in the c.m. frame, has some advantages over ordinary rapidity. In the c.m. frame, y is restricted at asymptotic s to the range $-\frac{1}{2}Y \leq y \leq +\frac{1}{2}Y$, where Y depends strongly on m and P_T^2, while y_r has the range $-1 \leq y_r \leq 1$ independent of m and P_T^2. This allows a simpler comparison to be made between different types of produced particles.

III. EXPERIMENTAL PROCEDURE

The data reported in this paper result from the analysis of approximately 150 000 pictures of $\pi^+ p$ interactions and approximately 90 000 pictures of $\pi^- p$ interactions in the BNL 80-inch hydrogen bubble chamber at 18.5-GeV/c incident beam momentum.[6] Details of the analysis are presented elsewhere.[7]

The film was double-scanned for all events with at least one visible V^0. The scanning efficiency for the $\pi^+ p$ sample was determined to be 97%; scanning efficiencies of 86% and 96% were determined for the zero-prong and non-zero-prong events, respectively, in the $\pi^- p$ sample. Approximately 30 000 V^0's were measured and then processed through the geometrical reconstruction program HGEOM and the kinematic fitting program GRIND, where four hypotheses were attempted: K_1^0, Λ^0, $\bar{\Lambda}^0$, and γ. Approximately 3% of the events were "unmeasurable." Events that failed to be reconstructed or to obtain a fit were remeasured. Approximately 10% of the events still failed in reconstruction or fitting after two measurements. Events with more than one kinematic fit were examined and fits inconsistent with observed ionization were eliminated.

The K_1^0's, Λ^0's, and $\bar{\Lambda}^0$'s were separately studied to take into consideration the loss of events due to undetected decays close to the production vertex and to decays outside the chamber. In order to correct for such losses, we define a minimum decay length of 0.4 cm and a fiducial volume in which the decay must occur. A weight was then calculated for each V^0. The resulting weights averaged approximately 1.13.

To investigate possible electron-pair contamination in the data, we examined the distributions of the square of the unfitted invariant mass M^2 calculated for the V^0's, assuming the decay tracks to be electrons. In all distributions we found evidence of contamination revealed by a narrow peak at $M^2 \approx 0$. This contamination was strongest in the Λ^0 and $\bar{\Lambda}^0$ samples, with, as would be expected, approximately equal numbers of misidentifications in each sample. To eliminate this contamination, events with small M^2 were removed.[8] We present in Table I the numbers of V^0's before and after imposing fiducial volume and M^2 requirements.

A number of V^0's are listed in Table I as ambiguous (i.e., kinematically consistent with more than one hypothesis). The following argument is useful in understanding the nature of the ambiguities, and shows that most of the ambiguous K_1^0-Λ^0 events are Λ^0's. Consider a sample of pure $K_1^0 \to \pi^+\pi^-$ decays. Now assume that the following fits are tried for these events: $K_1^0, \Lambda^0, \bar{\Lambda}^0$. All the events should fit the K_1^0 hypothesis. But some will also fit the Λ^0 and $\bar{\Lambda}^0$ hypotheses due to measurement error and kinematic ambiguity. The important point is that as many K_1^0-Λ^0 ambiguities as K_1^0-$\bar{\Lambda}^0$ ambiguities should occur due to the symmetry of the K_1^0 decay. In this experiment, the K_1^0-Λ^0 ambiguities are more than 3 times as fre-

TABLE I. Numbers of inclusive V^0 particles.

		Initial number of V^0's (unweighted)		Number of vees after fiducial volume and M^2 cuts (unweighted)		Final number of V^0's (weighted [a])	
		π^+p	π^-p	π^+p	π^-p	π^+p	π^-p
	K_1^0	3684	2855	3621	2723	4191.2	3155.2
	Λ^0	2117	1720	1919	1369	2531.4	1764.1
	$\bar{\Lambda}^0$	325	394	110	77	156.2	118.6
ambiguous	K_1^0-Λ^0	427	226	418	201	...	...
ambiguous	K_1^0-$\bar{\Lambda}^0$	155	64	128	55	...	...
ambiguous	K_1^0-γ	30	34	0	0	...	...
ambiguous	Λ^0-γ	51	52	0	0	...	...
ambiguous	$\bar{\Lambda}^0$-γ	54	51	0	0	...	...

[a] Weighted for escape probability and ambiguous events.

quent as the K_1^0-$\bar{\Lambda}^0$ ambiguities. Thus it is clear that the K_1^0-Λ^0 ambiguities are not predominantly K_1^0's; there are more Λ^0's faking K_1^0's than K_1^0's faking Λ^0's. This seems plausible since, because of the larger Q value, many K_1^0 decay products have momentum components transverse to the K_1^0 line of flight which are kinematically impossible for Λ^0 decay products.

A quantitative apportionment of the ambiguous V^0's has been made, based on the characteristics of the effective-mass-squared distributions and decay-angle distributions for unambiguous K_1^0's, Λ^0's, and $\bar{\Lambda}^0$'s. The following technique was used. Consider, for example, a sample of pure $\Lambda^0 \to p\pi^-$ decays. The effective-mass-squared (M^2) distribution calculated from measured momenta for these events is expected to be Gaussian in shape when the appropriate masses are assigned to the decay particles. If, however, these events are treated as K_1^0's and the positive decay product is assigned pion mass $m(\pi)$, the resulting M^2 distribution is typically smooth, broad, and not of

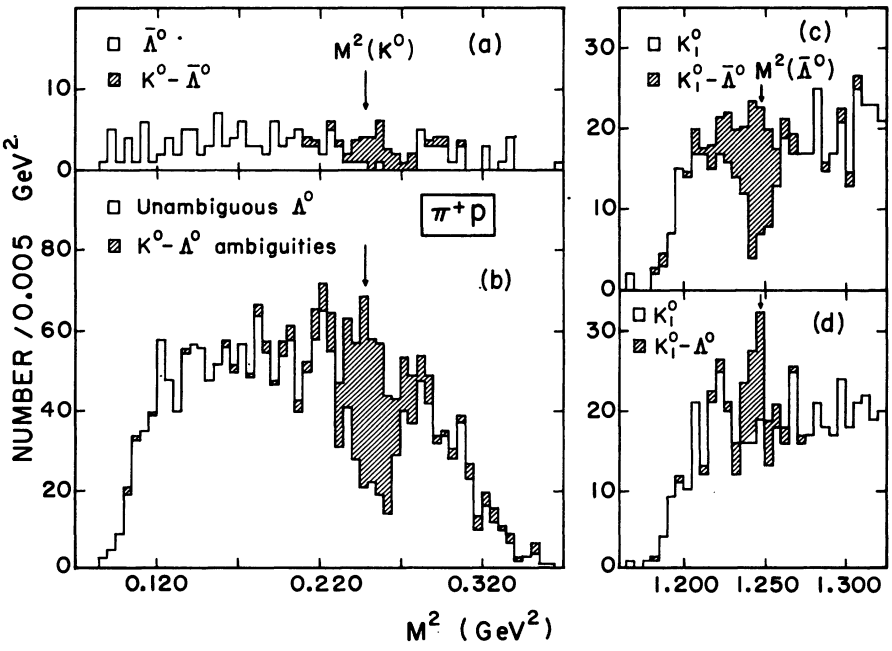

FIG. 1. M^2 distributions (with modified mass assignments for charged decay products as discussed in the text) for (a) $\bar{\Lambda}^0$ events, (b) Λ^0 events, and (c), (d) K_1^0 events in π^+p interactions. Unshaded events denote unambiguous V^0's while shaded events refer to ambiguous V^0's and are weighted as discussed in the text.

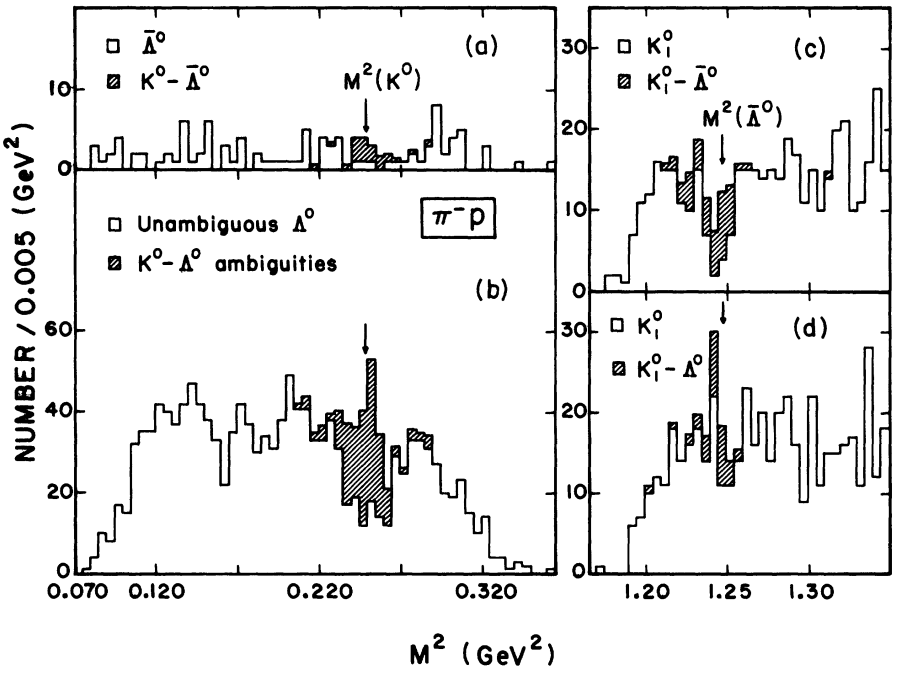

FIG. 2. M^2 distributions (with modified mass assignments for charged decay products as discussed in the text) for (a) $\bar{\Lambda}^0$ events, (b) Λ^0 events, and (c), (d) K_1^0 events in $\pi^- p$ interactions. Unshaded events denote unambiguous V^0's while shaded events refer to ambiguous V^0's which are weighted as discussed in the text.

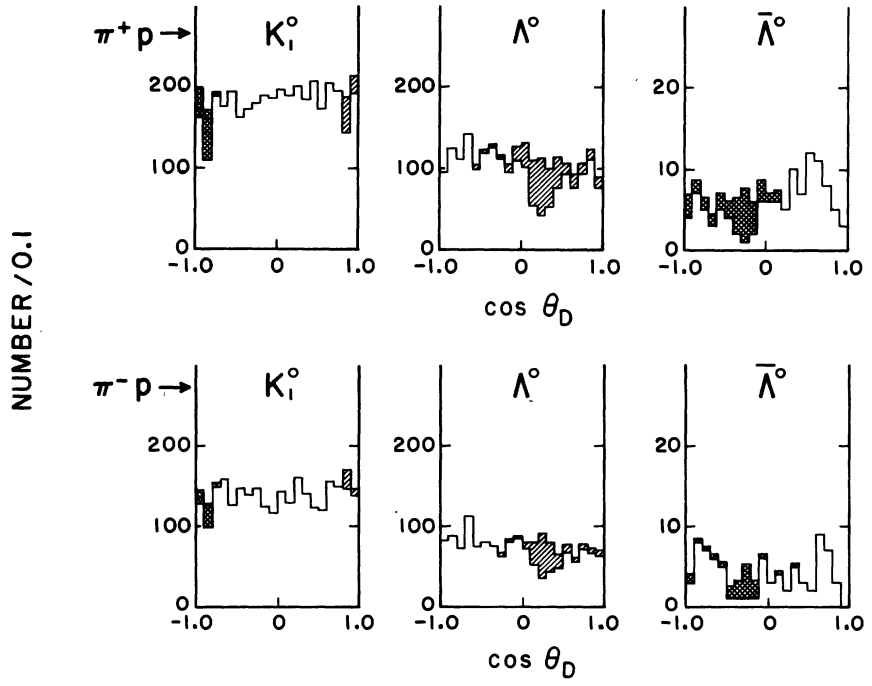

FIG. 3. Distributions of $\cos\theta_D$ (where θ_D is the angle between the momenta of the V^0 and of either decay product in the V^0 rest frame) for the K_1^0's, Λ^0's, and $\bar{\Lambda}^0$'s in the $\pi^+ p$ interactions. The unshaded distributions represent the ambiguous events. The cross-hatched events are the contributions from the K_1^0-$\bar{\Lambda}^0$ ambiguities while the single-slashed-line events represent the contributions from the K_1^0-Λ^0 ambiguities. The cross-hatched and single-slashed-line events are weighted as discussed in the text.

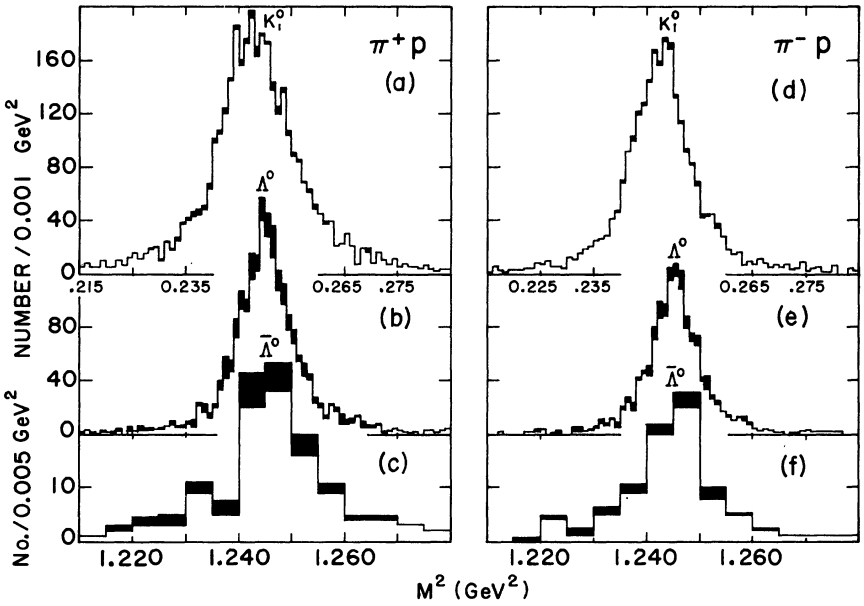

FIG. 4. The M^2 distributions (with correct mass assignments for the charged decay products) for (a) K_1^0, (b) Λ^0, and (c) $\bar{\Lambda}^0$ produced in the $\pi^+ p$ interactions and (d) K_1^0, (e) Λ^0, and (f) $\bar{\Lambda}^0$ produced in $\pi^- p$ interactions. Contributions from ambiguous V^0 events are shown shaded and are weighted as discussed in the text.

Gaussian shape. If the populated M^2 range for this distribution includes $m^2(K_1^0)$, some of the decays may be kinematically fitted as K_1^0 as well as Λ^0 and classified as ambiguous. Removal of these events from the sample would result in a dip centered at $m^2(K_1^0)$ in the M^2 distribution for events with unique Λ^0 fits treated as K_1^0's. Similar dips might be expected in the mass distributions for uniquely fitted K_1^0's incorrectly treated as Λ^0's or $\bar{\Lambda}^0$'s and for uniquely fitted $\bar{\Lambda}^0$'s incorrectly treated as K_1^0's.

In Figs. 1 and 2 we show (unshaded) the M^2 distributions for our unambiguous Λ^0, $\bar{\Lambda}^0$, and K_1^0 samples as calculated with $m(\pi)$ substituted for $m(p)$ or $m(\bar{p})$ in the Λ^0 and $\bar{\Lambda}^0$ samples, and $m(p)$ substituted for $m(\pi^+)$ or $m(\pi^-)$ in the K_1^0 sample. Dips are indeed seen at $m^2(K_1^0) = 0.248$ GeV^2 for the Λ^0 and $\bar{\Lambda}^0$ distributions and at $m^2(\Lambda^0) = 1.245$ GeV^2 for the K_1^0 distributions. By an iterative process we have determined what fractions of the corresponding M^2 distributions for ambiguous V^0's must be added to the M^2 distributions for unique V^0's to fill in these dips. The resulting contributions are shown shaded in Figs. 1 and 2. We estimate that 86% of the ambiguous K_1^0-Λ^0's are Λ^0's and that 14% are K_1^0's. Of the ambiguous K_1^0-$\bar{\Lambda}^0$ events we estimate that 75% are K_1^0's and 25% are $\bar{\Lambda}^0$'s. All distributions presented in the remainder of this paper will include contributions from the ambiguous events weighted by these percentages.

As a check on our apportionment of the ambiguous events we have examined the effect of their inclusion on the distributions of the decay angle, θ_D, of the K_1^0's, Λ^0's, and $\bar{\Lambda}^0$'s. The distributions of $\cos\theta_D$ (where θ_D is the angle between the momenta of the V^0 and of either decay product in the V^0 rest frame) should be isotropic unless events are lost or misidentified. (This is obviously true for the spinless K_1^0 and is true for the Λ^0 and $\bar{\Lambda}^0$ if there is no polarization along the line of flight.) Our $\cos\theta_D$ distributions are shown in Fig. 3 with the contributions of the ambiguous events shaded. We find that the distributions for the unambiguous events show deviations from isotropy. The addition of the contributions from the ambiguous events does indeed yield isotropic distributions.

In Fig. 4 are shown the M^2 distributions for the K_1^0's, Λ^0's, and $\bar{\Lambda}^0$'s (with correct mass assignments). Contributions from the ambiguous V^0's are shown shaded. The peaks are still seen to be Gaussian in shape with standard deviations of 0.013, 0.008, and 0.012 GeV^2 for the K_1^0's, Λ^0's, and $\bar{\Lambda}^0$'s produced in $\pi^+ p$ interactions, and 0.011, 0.007, and 0.011 GeV^2 for K_1^0's, Λ^0's, and $\bar{\Lambda}^0$'s produced in $\pi^- p$ interactions.

IV. CROSS SECTIONS AND MULTIPLICITIES

In order to study the data in terms of the scaling and limiting fragmentation hypotheses, accurate knowledge of absolute cross sections for the inclusive processes at each energy is required. Cross sections have been obtained in a consistent

TABLE II. Single strange-particle inclusive [a] cross sections.

Number of charged secondaries	σ (μb) for $\pi^+p \to$			σ (μb) for $\pi^-p \to$		
	K_1^0	Λ^0	$\bar{\Lambda}^0$	K_1^0	Λ^0	$\bar{\Lambda}^0$
0	...	...	...	63.9±12.9	58.0±12.1	5.2±2.0
2	307.1±21.3	233.0±18.0	15.7±2.4	502.4±34.8	266.0±23.0	30.0±4.5
4	507.3±34.0	321.0±24.0	21.0±2.4	633.3±43.0	385.9±32.0	18.2±6.6
6	267.0±10.0	144.0±12.0	6.6±1.4	327.4±23.8	176.2±16.0	8.4±2.2
8	51.0±5.0	33.6±4.0	0.9±0.5	53.8±6.2	31.8±4.7	...
10	4.0±1.0	2.8±1.0	...	7.3±2.0	3.9±1.4	...
Total	1136.4±73.0	734.4±53.0	44.2±3.4	1588.1±102.0	921.8±71.3	61.8±7.3
	$\sigma_{inel} = \sigma_T - \sigma_{el} = 19.68 \pm 0.77$ mb [b]			$\sigma_{inel} = \sigma_T - \sigma_{el} = 21.17 \pm 0.49$ mb [b]		

[a] Events with more than one V^0 are counted more than once in calculating these cross sections. The cross sections are corrected for neutral decay modes.
[b] See Ref. 1.

manner for reactions (1)–(6) by normalization to independent determinations of the 18.5-GeV/c π^+p and π^-p four-prong topological cross sections.[1,9] Corrections outlined in Sec. III have been applied. The cross sections for the different charge multiplicities are given in Table II. These cross sections have also been corrected for neutral decay modes.

We note that the K_1^0 cross sections for reaction (2) are always greater than the corresponding cross sections for reaction (1). Although the Λ^0 cross sections for reactions (3) and (4) appear equal within errors for any given multiplicity, the total cross section for reaction (4) is greater than that for reaction (3).

In Fig. 5 the fractions of the total inelastic cross section ($\sigma_T - \sigma_{el}$) contributed by events in which a K_1^0, Λ^0, or $\bar{\Lambda}^0$ is produced are plotted as a function of the charge multiplicity of the production vertex. The corresponding fractions for all events of a given charge multiplicity are indicated for comparison by the dashed curve. It is interesting to note that the ratios are the same within errors for reactions (1) and (2) (except for two-prong events) and are also the same within errors for reactions (3) and (4). It is also evident that the dashed curve is similar in shape to the curves for strange-particle data. This is true even for $\bar{\Lambda}^0$ production, where one might naively have expected the distribution to peak at higher multiplicities.

V. INCLUSIVE DISTRIBUTIONS

In this section we present and discuss the inclusive distributions for reactions (1)–(6), in terms of the variables defined in Sec. II. In Sec. V A the features of the longitudinal-momentum distributions are presented in terms of the variables x, y, y_r, and P_L, and qualitative comparisons are made with the corresponding strange-particle inclusive spectra from K^+p,[10] K^-p,[11] pp,[12] and $\bar{p}p$[13] reactions. In Sec. V B the P_T^2 distributions are examined, fits are presented, and the average transverse momenta of the reactions are discussed. In Sec. V C the Λ^0 polarization in these inclusive reactions is presented.

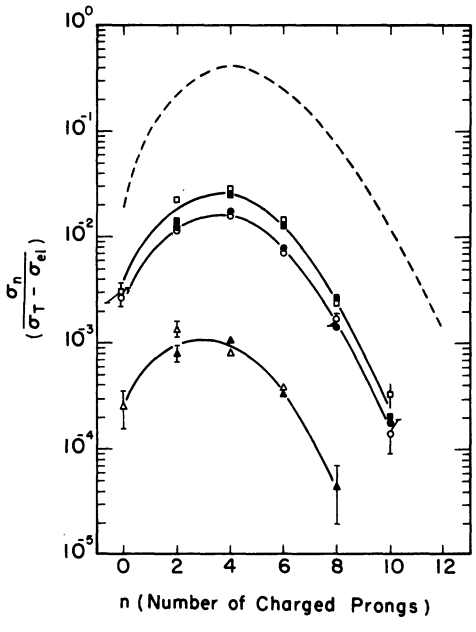

FIG. 5. Fractions of the total inelastic cross section ($\sigma_T - \sigma_{el}$) are shown as a function of the charge multiplicity of the production vertex for K_1^0 (□), Λ^0 (○), and $\bar{\Lambda}^0$ (△) in π^-p interactions, and K_1^0 (■), Λ^0 (●), and $\bar{\Lambda}^0$ (▲) in π^+p interactions. The corresponding fractions for all events are indicated for comparison by the dashed curve. The other curves are hand drawn to show the general features of the distributions.

A. Inclusive longitudinal-momentum distributions

Figure 6 shows distributions of

$$F_1(x) = \int_{\text{all } P_T^2} f(x, P_T^2) dP_T^2$$

for reactions (1)–(6), where

$$f(x, P_T^2) = \frac{2E^*}{\pi\sqrt{s}} \frac{d^2\sigma}{dx dP_T^2}$$

is the invariant differential cross section. The general features are strongly dependent upon the type of particle produced. The K_1^0 distributions are not symmetric about $x = 0$. More K_1^0's are produced in the forward hemisphere, suggestive of beam fragmentation. In contrast the Λ^0 events are concentrated largely in the backward hemisphere, suggestive of target fragmentation. The $\bar{\Lambda}^0$ distributions are significantly different from the Λ^0 distributions. They appear consistent either with beam fragmentation or with production in the central region independent of beam or target.

Distributions of the cosine of the c.m. production angle θ^* for K_1^0's, Λ^0's, and $\bar{\Lambda}^0$'s, shown in Fig. 7, support the hypothesis that $\bar{\Lambda}^0$'s are produced in the central region. While the distributions for K_1^0's and Λ^0's are peaked, respectively, forward and backward, the $\bar{\Lambda}^0$ distributions are symmetric and contain a relatively smaller fraction of events in the peaks near $|\cos\theta^*| = 1$.

It is interesting that the ratio of the cross section for reaction (4) to that for reaction (3) in the target-fragmentation region is inconsistent with the value ≈10 predicted[14] by pole factorization, given the corresponding cross section for the reaction $K^- p \to \Lambda^0 + \text{anything}$.

In Fig. 8 the x distributions for reactions (1) and (2) are compared with x distributions for the re-

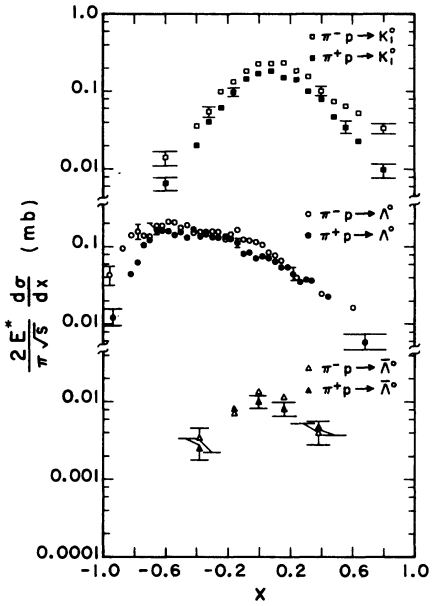

FIG. 6. Distributions of $(2E^*/\pi\sqrt{s})d\sigma/dx = F_1(x) = \int_{\text{all } P_T^2} f(x, P_T^2) dP_T^2$ as a function of x for reactions (1)–(6).

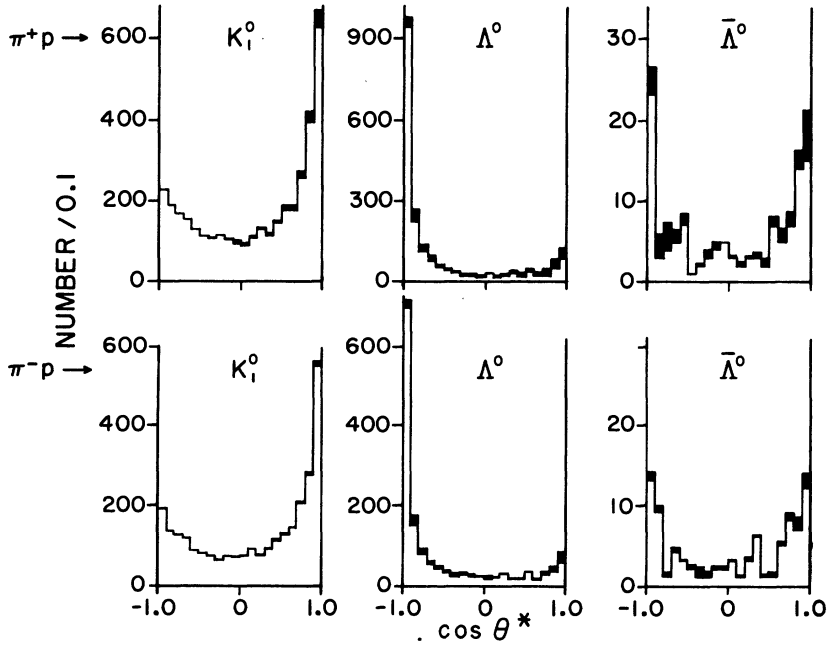

FIG. 7. Distributions of the cosine of the c.m. production angle θ^* for the K_1^0's, Λ^0's, and $\bar{\Lambda}^0$'s for the $\pi^+ p$ and $\pi^- p$ data. Contributions from the ambiguous V^0's are shown shaded.

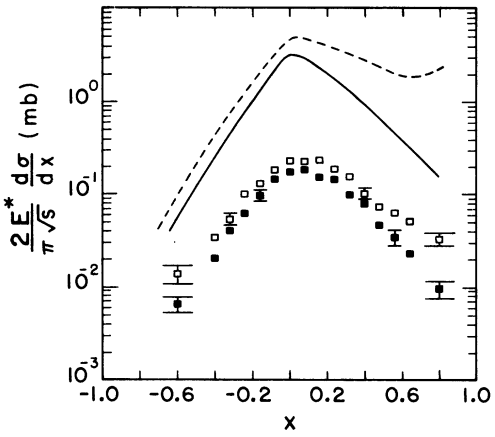

FIG. 8. Distributions of $(2E^*/\pi\sqrt{s})d\sigma/dx = F_1(x) = \int_{\text{all } P_T^2} f(x, P_T^2) dP_T^2$ as a function of x for the reactions $\pi^+ p \to K_1^0$ + anything (■), $\pi^- p \to K_1^0$ + anything (□), $\pi^+ p \to \pi^-$ + anything (solid line), $\pi^- p \to \pi^-$ + anything (dashed line), all at 18.5-GeV/c incident momentum.

actions

$$\pi^+ p \to \pi^- + \text{anything} \tag{7}$$

and

$$\pi^- p \to \pi^- + \text{anything} \tag{8}$$

at the same incident momentum. We note that the differences in the distributions for reactions (1) and (2) are qualitatively similar to the differences seen in the distributions for reactions (7) and (8). Similarities in shape are seen in the distributions for reactions (1) and (7) and reactions (2) and (8). In both cases the π^--induced reaction has a larger cross section and exhibits more asymmetry in the x distribution.

To examine the projectile dependence of K_1^0 production, distributions of

$$\int_{\text{all } P_T^2} \frac{E^*}{\pi} \frac{d^2\sigma}{dP_L^* dP_T^2} dP_T^2,$$

for reactions (1) and (2) and for the reactions

$$K^- p \to K_1^0 + \text{anything} \quad \text{at 12.6 GeV}/c,^{11} \tag{9}$$

$$K^+ p \to K_1^0 + \text{anything} \quad \text{at 12.7 GeV}/c,^{10} \tag{10}$$

and

$$pp \to K_1^0 + \text{anything} \quad \text{at 19 GeV}/c,^{12} \tag{11}$$

are presented in Fig. 9(A).

We note that in the backward ($x < 0$) direction, the shapes of the distributions for incident pions, protons, and kaons are very similar. Regge factorization suggests that at sufficiently high energies these distributions might be the same in magnitude as well as when they are appropriately normalized. The recent CERN ISR results, which show an increase at high energy in pp total cross sections, make normalizing to "$\sigma(\text{tot})_\infty$" difficult. In any case, dividing the distributions by values of "$\sigma(\text{tot})_\infty$" used in similar analyses has the effect of changing the ordering of the data but does not bring them into better agreement. It is clear that factorization is not exact at these energies. As might be expected, the differences in both shape and magnitude are greater in the forward direction for the different beam particles.[15]

In Fig. 9(B) is shown the invariant cross section as a function of x for Λ^0 production for our data [reactions (3) and (4)] along with that for the reactions

$$K^- p \to \Lambda^0 + \text{anything} \quad \text{at 12.6 GeV}/c,^{11} \tag{12}$$

$$K^+ p \to \Lambda^0 + \text{anything} \quad \text{at 12.7 GeV}/c,^{10} \tag{13}$$

$$pp \to \Lambda^0 + \text{anything} \quad \text{at 19 GeV}/c,^{12} \tag{14}$$

and

$$\bar{p}p \to \Lambda^0 + \text{anything} \quad \text{at 5.7 GeV}/c.^{13} \tag{15}$$

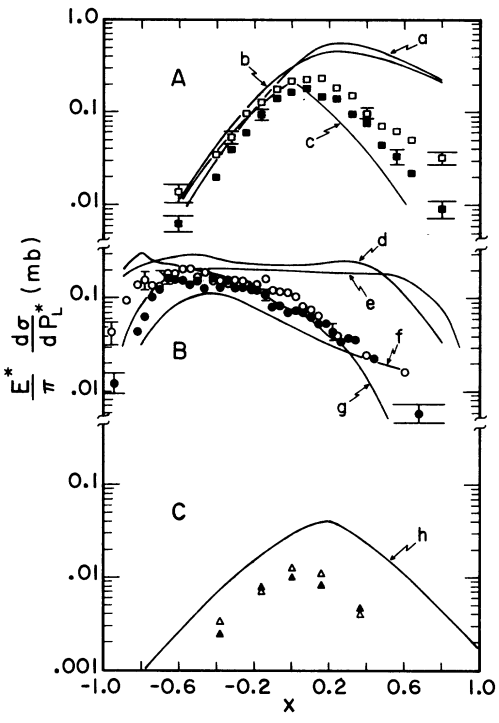

FIG. 9. (A) Distributions of $(E^*/\pi)d\sigma/dP_L^*$ as a function of x for reactions (1) (■) and (2) (□). The solid curves show the corresponding distributions for (a) $K^- p \to K_1^0$ + anything at 12.6 GeV/c, (b) $K^+ p \to K_1^0$ + anything at 12.7 GeV/c, and (c) $pp \to K_1^0$ + anything at 19 GeV/c. (B) Distributions of $(E^*/\pi)d\sigma/dP_L^*$ as a function of x for reactions (3) (●) and (4) (○). The solid curves show the corresponding distributions for (d) $K^- p \to \Lambda^0$ + anything at 12.6 GeV/c, (e) $pp \to \Lambda^0$ + anything at 19 GeV/c, (f) $K^+ p \to \Lambda^0$ + anything at 12.7 GeV/c, and (g) $\bar{p}p \to \Lambda^0$ + anything at 5.7 GeV/c. (C) Distributions of $(E^*/\pi)d\sigma/dP_L^*$ as a function of x for reactions (5) (▲), and (6) (△), and for $K^+ p \to \bar{\Lambda}^0$ + anything at 12.7 GeV/c (solid curve h).

One might naively expect these distributions to be very similar for $x<0$ since, in each case, one is observing proton fragmentation into Λ^0 +anything. For $x<-0.6$, however, the distributions are quite different in magnitude and, more significantly, in shape. Note, for example, the significant difference in the distributions for reaction (3) and (4) beginning at $x\approx -0.7$. We find, however, that this difference disappears if one adopts a procedure for removing quasi-two-body events[16] from the $\pi^- p$ data. (Quasi-two-body final states heavily populate the zero- and two-prong data for $\pi^- p$ collisions but not for $\pi^+ p$ collisions.) It has been reported[13] that removing quasi-two-body events in reaction (15) also has the effect of eliminating the peak at $x=-0.8$. It is interesting to speculate that the differences in shape among the distributions in the region of large negative x for all the reactions included in Fig. 9(B) are attributable to quasi-two-body processes, which tend to be relatively more important at lower energies, and that these distributions will in fact become more and more alike as s increases.

The production of Λ^0's is remarkably similar for four of the six reactions ($\pi^+ p$, $\pi^- p$, $K^+ p$, and $\bar{p}p$) in the region $-0.4\lesssim x\lesssim 0.4$. In this region, quasi-two-body reactions do not dominate. From this we infer that the mechanism of Λ^0 production is inherently different in $K^- p$ and pp reactions than in the other four reactions.

Finally in Fig. 9(C) a comparison is made between reactions (5) and (6) and

$$K^+ p \to \bar{\Lambda}^0 + \text{anything} \quad \text{at } 12.7 \text{ GeV}/c.^{10} \tag{16}$$

The $\bar{\Lambda}^0$ spectrum from the $K^+ p$ reaction is similar in shape to those from the $\pi^+ p$ and $\pi^- p$ reactions, although its magnitude is significantly larger.

In Fig. 10 are shown distributions of the function[17]

$$G_1(y)=\int_{\text{all } P_T^2} f(y,P_T^2)\,dP_T^2,$$

with

$$f(y,P_T^2)=\frac{1}{\pi}\frac{d^2\sigma}{dy\,dP_T^2}\ .$$

We notice even at our energy what may be the onset of a plateau in the rapidity plot for K_1^0 production.

We present the inclusive distributions in terms of the reduced rapidity y_r for reactions (1)–(6) in Fig. 11. Here we define the structure function

$$R_1(y_r)=\int_{\text{all } P_T^2} f(y_r,P_T^2)\,dP_T^2,$$

with

$$f(y_r,P_T^2)=\frac{2}{\pi Y}\frac{d^2\sigma}{dy_r\,dP_T^2}\ .$$

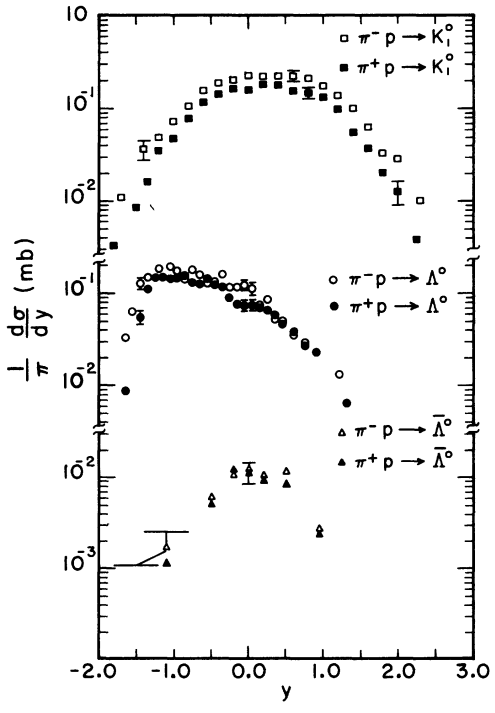

FIG. 10. Distributions of $(1/\pi)(d\sigma/dy)=G_1(y)$ $=\int_{\text{all}P_T^2} f(y,P_T^2)dP_T^2$ as a function of y for reactions (1)–(6).

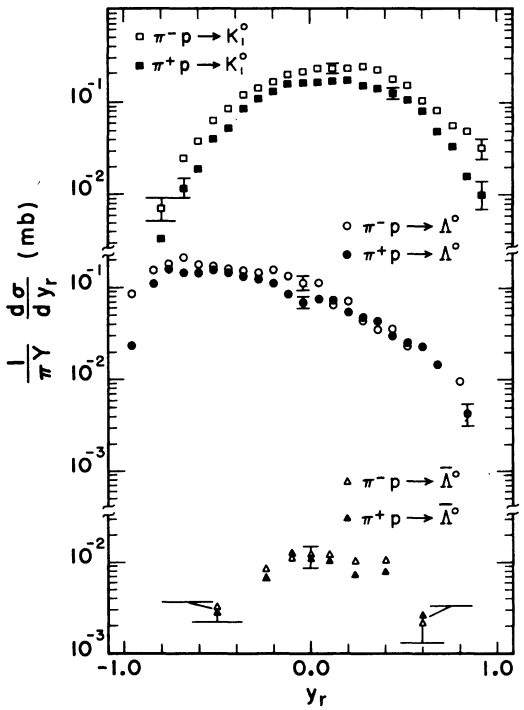

FIG. 11. Distributions of $(1/\pi Y)(d\sigma/dy_r)=R_1(y_r)$ $=\int_{\text{all}P_T^2} f(y_r,P_T^2)dP_T^2$ as a function of y_r for reactions (1)–(6).

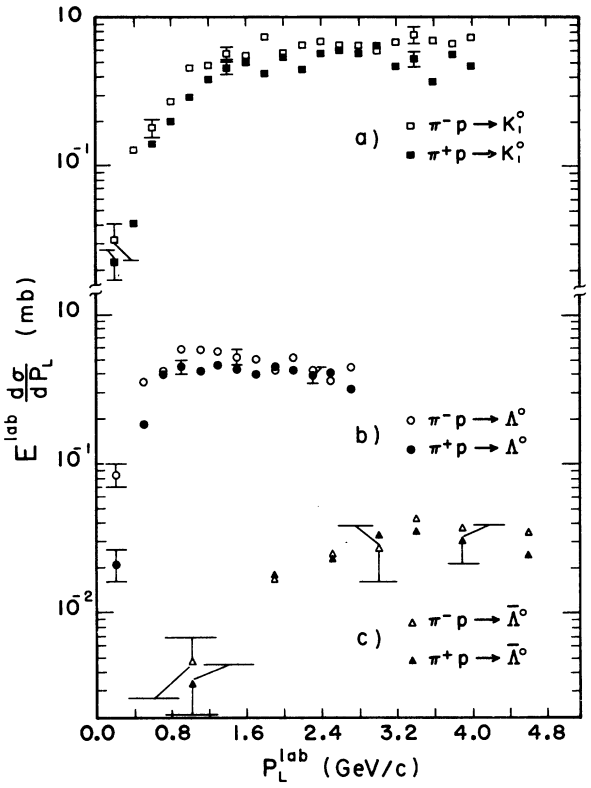

FIG. 12. Distributions of

$$E^{lab}\frac{d\sigma}{dP_L} = H_1(P_L) = \int_{\text{all } P_T^2} E^{lab}\frac{d^2\sigma}{dP_L dP_T^2}\,dP_T^2$$

as a function of P_L for reactions (1)–(6).

These distributions show the same features discussed above. However, the limits of the distribution are now independent of m and P_T^2.

In Fig. 12 the longitudinal-momentum distributions for reactions (1)–(6) are presented in the target (lab) frame. The distributions shown are defined in terms of the function

$$H_1(P_L) = \int_{\text{all } P_T^2} E^{lab}\frac{d^2\sigma}{dP_L dP_T^2}\,dP_T^2 .$$

The effects observed in these distributions, in which the extreme backward region is shown in greater detail, have been discussed above in terms of the c.m. longitudinal variables.

B. Inclusive P_T^2 distributions and mean transverse momenta

The transverse-momentum distributions for reactions (1)–(6) are presented in Fig. 13 as a function of the quantity

$$H_2(P_T^2) = \int_{\text{all } P_L} E^{lab}\frac{d^2\sigma}{dP_T^2 dP_L}\,dP_L ,$$

and in Fig. 14 as a function of the quantity

$$H_3(P_T^2) = \int_{\text{all } P_L} \frac{d^2\sigma}{dP_T^2 dP_L}\,dP_L .$$

These distributions were fitted with the exponential functions of P_T^2 shown in Table III. We see that acceptable fits were obtained to all data. We notice that the values of the parameter b are the same within errors for reactions (1) and (2), reactions (3) and (4), and reactions (5) and (6). Thus the slope shows no significant variation with incident charge for $P_T^2 \leq 1.0$ (GeV/c)^2. In pp collisions at 205 GeV/c the slope of $d\sigma/dP_T^2 \sim e^{(-bP_T^2)}$ for K_1^0's[18] was found to be equal to 4.4 ± 1.6 GeV^{-2}, consistent within errors with our value. For Λ^0's they found $b = 2.8 \pm 0.8$ GeV^{-2}, again within errors of our value.

Most theories or models dealing with inclusive reactions assume that the average transverse momentum of the produced inclusive particle is independent of incident energy, of incident particle, and of the produced inclusive particle. This is done in order to be able to reduce the complexity of the problem by ignoring the transverse momen-

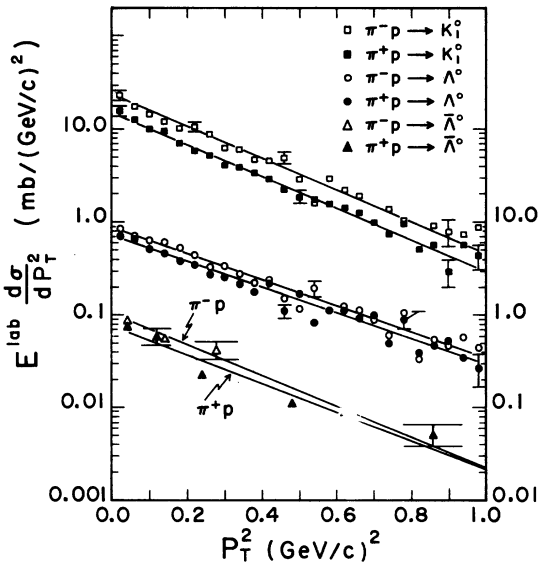

FIG. 13. Distributions of

$$E^{lab}\frac{d\sigma}{dP_T^2} = H_2(P_T^2) = \int_{\text{all } P_L} E^{lab}\frac{d^2\sigma}{dP_T^2 dP_L}\,dP_L$$

as a function of P_T^2 for reactions (1)–(6). The solid lines represent fits to the function $Ae^{-BP_T^2}$. The scale on the left of the figure is for the K_1^0 distribution only, while the scale on the right is for the Λ^0 and $\bar{\Lambda}^0$ distributions.

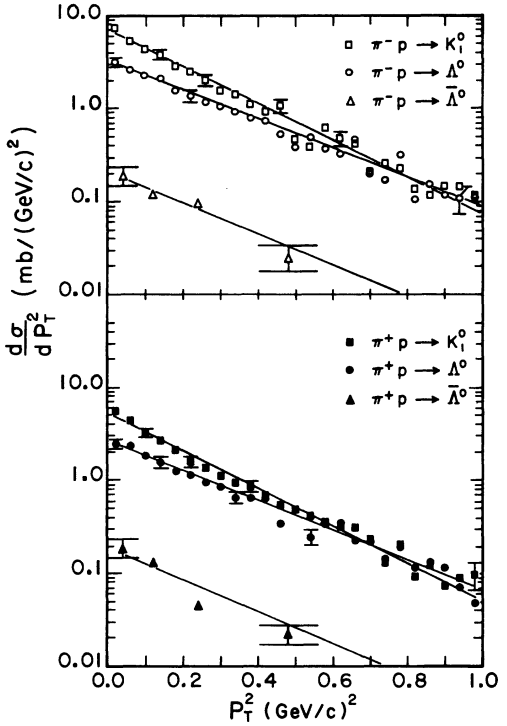

FIG. 14. Distributions of

$$\frac{d\sigma}{dP_T{}^2} = H_3(P_T{}^2) = \int_{\text{all}P_L} \frac{d^2\sigma}{dP_T{}^2 dP_L}\, dP_L$$

as a function of $P_T{}^2$ for reactions (1)–(6). The solid lines represent fits to the function $ae^{-bP_T{}^2}$

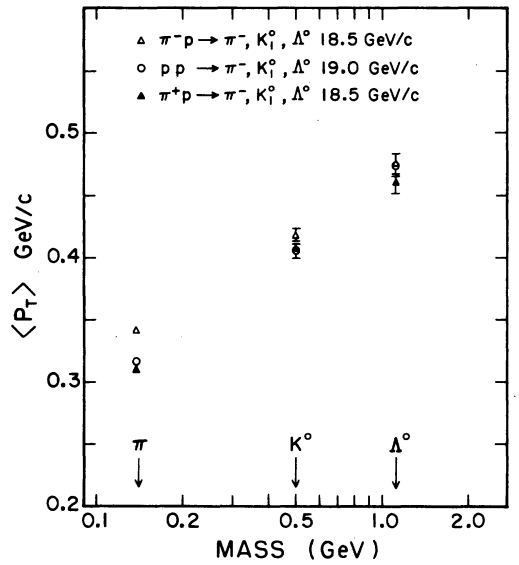

FIG. 15. Values of the average transverse momentum as a function of mass for the produced particles, π^-, K_1^0, and Λ^0, in 18.5-GeV/c $\pi^+ p$ and $\pi^- p$ interactions and in 19-GeV/c pp interactions.

tum. Evidence from a previous study,[12] combined with our results, indicates that in fact the average transverse momentum depends on all three of these variables.

In Fig. 15 the average transverse momentum is presented as a function of mass for the produced inclusive particles, π^-, K_1^0, and Λ^0, for the 18.5-GeV/c $\pi^+ p$ and $\pi^- p$ data and for the 19-GeV/c pp data.[12] The value of $\langle P_T \rangle$ appears to increase logarithmically with the mass of the produced inclusive particle. In addition, $\langle P_T \rangle$ is consistently higher in $\pi^- p$ interactions than in $\pi^+ p$ interactions for these produced particles. In Fig. 16 mean transverse momenta for the K_1^0, Λ^0, $\bar{\Lambda}^0$ are presented as a function of charge multiplicity at the production vertex. The $\langle P_T \rangle$ values for $\pi^- p$ interactions are generally higher than the values for $\pi^+ p$ interactions for each charge multiplicity. For the K_1^0 sample, the average transverse momentum decreases as the charge multiplicity increases. This is similar to the decrease in $\langle P_T \rangle$ with increasing multiplicity seen for produced π^-. In contrast the Λ^0 and $\bar{\Lambda}^0$ samples show no significant variation in $\langle P_T \rangle$ with charge multiplicity.

C. Λ^0 polarization

We have studied the polarization of the $\Lambda^0(\Sigma^0)$ inclusive spectra. The polarization P is measured along the normal to the plane containing the momenta of the Λ^0 and the initial pion. The polarizations have been determined from fits of the form $(1 + \alpha P \cos\theta)$ to distributions of $dN/d(\cos\theta_P)$, with

TABLE III. Parameters for the fits $d\sigma/dP_T{}^2 = ae^{-bP_T{}^2}$ and $E^{\text{lab}} d\sigma/dP_T{}^2 = Ae^{-BP_T{}^2}$.

Reaction	a [mb/(GeV/c)^2]	b [(GeV/c)$^{-2}$]	Confidence level	A [mb/(GeV/c^2)]	B [(GeV/c)$^{-2}$]	Confidence level
$\pi^+ p \to K_1^0$	5.12 ± 0.19	4.60 ± 0.10	20%	15.54 ± 0.59	3.96 ± 0.10	65%
$\to \Lambda^0$	2.74 ± 0.12	3.72 ± 0.12	35%	7.31 ± 0.32	3.21 ± 0.12	5%
$\to \bar{\Lambda}^0$	0.19 ± 0.02	3.96 ± 0.35	2%	0.78 ± 0.10	3.59 ± 0.36	4%
$\pi^- p \to K_1^0$	7.16 ± 0.26	4.59 ± 0.11	3%	23.31 ± 0.86	3.91 ± 0.11	1%
$\to \Lambda^0$	3.28 ± 0.16	3.62 ± 0.13	65%	8.77 ± 0.43	3.24 ± 0.13	50%
$\to \bar{\Lambda}^0$	0.22 ± 0.03	3.95 ± 0.46	60%	1.02 ± 0.17	3.79 ± 0.54	40%

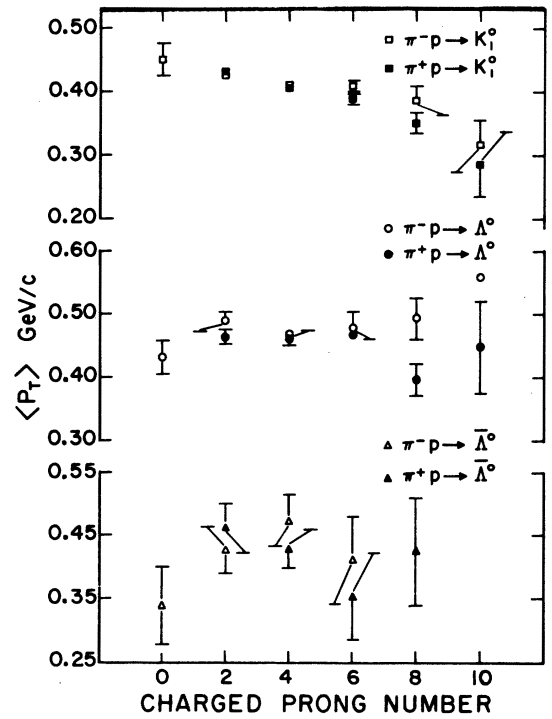

FIG. 16. Values of the average transverse momentum for the produced particles K_1^0, Λ^0, and $\bar{\Lambda}^0$ in 18.5-GeV/c $\pi^+ p$ and $\pi^- p$ interactions as a function of charge multiplicity at the production vertex.

α assumed[19] to be +0.645. The polarization angle θ_p is thus defined as

$$\cos\theta_p = \frac{(\vec{\pi}\times\vec{\Lambda})\cdot\vec{p}}{|\vec{\pi}\times\vec{\Lambda}|\,|\vec{p}|}\ ,$$

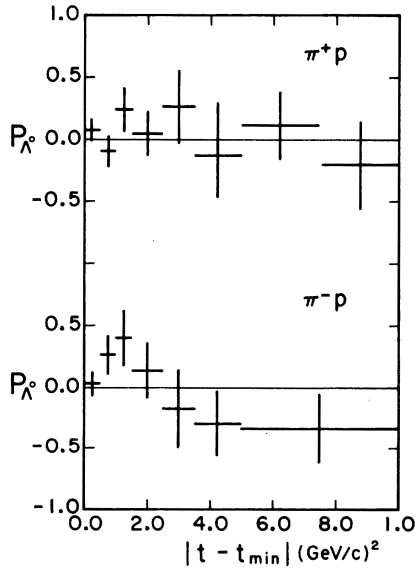

FIG. 17. Distributions of the Λ^0 polarization as a function of $|t - t_{min}|$ in 18.5-GeV/c $\pi^+ p$ and $\pi^- p$ interactions.

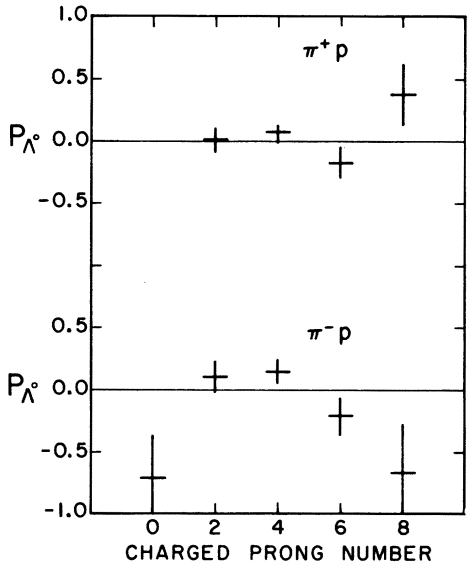

FIG. 18. Distributions of the Λ^0 polarization as a function of charge multiplicity at the production vertex in 18.5-GeV/c $\pi^+ p$ and $\pi^- p$ interactions.

with $\vec{\pi}$ = incident $\pi^\pm$ momentum, $\vec{\Lambda}$ = Λ^0 momentum in the over-all c.m. system, and $\vec{p}$ = momentum of the proton from decay of Λ^0 in the Λ^0 c.m. system.

In Fig. 17 we present values for the polarization as a function of $|t - t_{min}|$, where t is the square of the four-momentum transfer from the target proton to the Λ^0 and t_{min} is the minimum possible value of t calculated for each event. We see significant

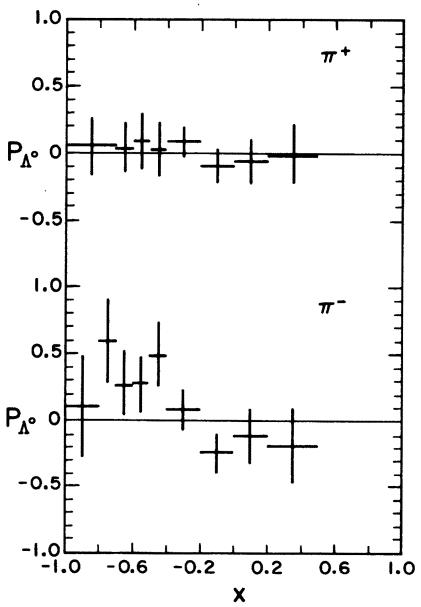

FIG. 19. Distributions of the Λ^0 polarization as a function of the scaling variable x in 18.5-GeV/c $\pi^+ p$ and $\pi^- p$ interactions.

differences between the polarizations for π^+p and π^-p interactions. The π^+p polarization is everywhere consistent with zero, while the π^-p polarization exhibits a positive peak at low $|t-t_{\min}|$ and shows a negative trend for large $|t-t_{\min}|$.

In Fig. 18 we show the polarization as a function of the number of charged prongs at the production vertex. The positive polarization observed for π^-p interactions appears to be primarily due to two- and four-prong interactions. The effect is apparently not due to Λ^0+K^0 production, since the polarization for zero-prong interactions is negative. A negative polarization is also observed for events with high charge multiplicity at the primary vertex. However, the cross sections are smaller (see Table II) for the charge multiplicities showing negative polarization.

Finally, in Fig. 19 we present the polarization as a function of the scaling variable x. We again see that the Λ^0 polarization from π^+p events is everywhere consistent with zero while the polarization from π^-p events is positive in the target-fragmentation region. This contrasts with results from K^-p interactions[20,21] which show zero polarization in the backward hemisphere and a negative polarization in the forward hemisphere. Polarization for Λ^0's produced in $p\bar{p}$ interactions[22] is consistent with zero for all values of $|t|$.

ACKNOWLEDGMENTS

We would like to thank the staffs of the 80-in. bubble chamber and the AGS at Brookhaven National Laboratory for their cooperation. The efforts of W. L. Rickhoff, R. L. Erichsen, and the Notre Dame scanning and measuring staff are acknowledged with appreciation.

---

*Work supported in part by the National Science Foundation.

†Submitted in partial fulfillment of the requirements for the Ph.D. degree at the University of Notre Dame.

[1]J. T. Powers *et al.*, Phys. Rev. D 8, 1947 (1973). See also: N. N. Biswas *et al.*, Phys. Rev. Lett. 26, 1589 (1971); W. D. Shephard *et al.*, *ibid.* 27, 1164 (1971); 28, 260(E) (1972); 28, 703 (1972); M. Alston-Garnjost *et al.*, Phys. Lett. 39B, 402 (1972).

[2]We are unable to distinguish between a Λ^0 which is produced directly in the primary interaction and one that results from decay of a Σ^0.

[3]D. J. Crennell *et al.*, Phys. Rev. Lett. 28, 643 (1972).

[4]A V^0 is the characteristic two-track pattern formed by the visible (i.e., charged-mode) decay of a neutral strange particle.

[5]W. R. Fraser *et al.*, Rev. Mod. Phys. 44, 284 (1972).

[6]The π^+ incident momentum was measured to be 18.465 $\pm$ 0.092 GeV/c, while the π^- incident momentum was measured to be 18.480 $\pm$ 0.092 GeV/c.

[7]P. H. Stuntebeck, doctoral thesis, University of Notre Dame, 1973 (unpublished).

[8]For the K_1^0 and Λ^0 samples all V^0's with $M^2 \leq 0.001$ GeV^2 were deleted from the final sample. Because of the smaller signal-to-noise ratio in the $\bar{\Lambda}^0$ sample, V^0's with $M^2 \leq 0.006$ GeV^2 were deleted.

[9]J. T. Powers, doctoral thesis, University of Notre Dame, 1972 (unpublished).

[10]S. Stone *et al.*, Phys. Rev. D 5, 1621 (1972).

[11]T. Ferbel, University of Rochester Report No. UR-408 (unpublished); rapporteur talk at The Third International Colloquium on Multiparticle Reactions, Zakopane, Poland, 1972 (unpublished).

[12]H. Bøggild *et al.*, Nucl. Phys. B57, 77 (1973).

[13]S. N. Ganguli and B. Sadoulet, Nucl. Phys. B53, 458 (1973).

[14]H. I. Miettinen, doctoral thesis, presented to the Philosophical Faculty at the University of Helsinki (unpublished).

[15]We note, however, that when low-multiplicity (zero-prong and two-prong) events are removed from reactions (1) and (2), the difference in slope of the x distributions for $x > 0$ is eliminated.

[16]We removed all zero-prong events and all two-prong events for which the square of the mass recoiling against the Λ^0 was less than 10 GeV^2. This value was selected as the cutoff because the most massive reported K^* resonance is the $K_N(3000)$.

[17]Symbols for the various structure functions used in this paper are chosen to agree with those used previously in Ref. 1.

[18]G. R. Charlton *et al.*, quoted by P. Söding, in *Proceedings of the XVI International Conference on High Energy Physics, Chicago-Batavia, Ill., 1972,* edited by J. D. Jackson and A. Roberts (NAL, Batavia, Ill., 1973), Vol. 1, p. 316.

[19]Particle Data Group, Phys. Lett. 39B, 1 (1972).

[20]W. Barletta *et al.*, Nucl. Phys. B51, 499 (1973).

[21]J. Bartsch *et al.*, Nucl. Phys. B40, 103 (1972).

[22]B. Y. Oh and G. A. Smith, Nucl. Phys. B49, 13 (1972).